

Halo Radius (Splashback Radius) of Groups and Clusters of Galaxies on Small Scales

F. G. Kopylova^{1,*} and A. I. Kopylov^{1,**}

¹*Special Astrophysical Observatory of the Russian AS, Nizhnij Arkhyz 369167, Russia*

We report the results of a study of the distribution of galaxies in the projection along the radius ($R \leq 3R_{200c}$) for 157 groups and clusters of galaxies in the local Universe ($0.01 < z < 0.10$) with line-of-sight velocity dispersions $200 \text{ km s}^{-1} < \sigma < 1100 \text{ km s}^{-1}$. We introduce a new observed boundary for the halos of clusters of galaxies, which we identify with the splashback radius R_{sp} . We also identified the core of groups/clusters of galaxies with the radius R_c . These radii are determined by the observed integrated distribution of the number of galaxies as a function of squared angular radius from the center of the group/cluster, which (usually) coincides with the brightest galaxy. We found for the entire sample that the boundary of dark matter R_{sp} for groups/clusters of galaxies is proportional to the radius R_{200} of the virialized region. We measured the mean radius $\langle R_{\text{sp}} \rangle = 1.14 \pm 0.02 \text{ Mpc}$ for groups of galaxies ($\sigma \leq 400 \text{ km s}^{-1}$) and $\langle R_{\text{sp}} \rangle = 2.00 \pm 0.07 \text{ Mpc}$ for clusters of galaxies ($\sigma > 400 \text{ km s}^{-1}$). The mean ratio of radii is $\langle R_{\text{sp}}/R_{200c} \rangle = 1.40 \pm 0.02$, or $\langle R_{\text{sp}}/R_{200m} \rangle = 0.88 \pm 0.02$.

Keywords: galaxies: groups and clusters: general—galaxies: evolution—cosmology: large-scale structure of the Universe

1. INTRODUCTION

Clusters of galaxies are the biggest gravitationally bound objects in the Universe. They are collapsed structures, which are viewed as a dark-matter halo. Clusters of galaxies increase their mass as a result of impacts of galaxies and smaller groups of galaxies along the filaments, and as a result of continuous infall of dark-matter objects. They have no clear boundaries and their boundaries are defined based on the density contrast with respect to the critical or mean density of the Universe. The evolution of clusters of galaxies is analyzed in terms of the spherical collapse model in expanding Universe (Gunn and Gott 1972; Gott 1973). In this model the system of galaxies virializes in several oscillations: maximum compression is followed by the next, secondary compression. Of special interest are the region of clusters of galaxies where the model dark-matter particles (galaxies) from filaments occur that fall for the first time onto the cluster and the collapsing spherical halo. The N -body simulations of the motion of the dark-matter halo (galaxies) performed by Balogh et al. (2000); Mamon et al. (2004); Gill et al. (2005)

revealed that a substantial fraction of such particles (up to 50%) located outside virialized regions of galaxy clusters (out to $2R_{\text{vir}}$ or $2R_{200c}$ ¹) has already been inside the region defined by these boundaries. These are the so-called “backsplash” galaxies, which have once passed the pericenter of their orbit during the gravitational collapse and which will return there again after reaching the apocenter. Haines et al. (2015) reports the results of Millennium simulations for 75 galaxy clusters at $z = 0.0$ and shows that a substantial fraction of “backsplash” galaxies “rebounds” out to $3r_{\text{proj}}/r_{200}$ on the phase diagram. Pimblet (2010) determined the fraction of “backsplash” galaxies inside $1\text{--}2R_{\text{vir}}$ based on their analysis of the SDSS catalog and simulations of 14 galaxy clusters.

Adhikari et al. (2014) introduced the radius of a galaxy cluster (the physical halo boundary), the splashback radius R_{sp} , as the radius where the recently accreted dark-matter halos pile up within the apocenters of their orbits. According

¹ Here R_{200c} (hereafter R_{200}) is the cluster radius inside which the density exceeds the critical density of the Universe by a factor of 200. In our studies it is determined by the dispersion of line-of-sight velocities of galaxies in clusters. In simulations another radius— R_{200m} —is often used, inside which the density exceeds the average density of the Universe by a factor of 200.

* Electronic address: flera@sao.ru

** Electronic address: akop@sao.ru

to the results of the N -body simulations of (Adhikari et al. 2014; Diemer and Kravtsov 2014) the R_{sp} radius shows up conspicuously by the sharp decrease on the composite density profile of the dark-matter halo. The simulations performed by More et al. (2015) showed that the location of R_{sp} depends on the mass accretion rate: $R_{\text{sp}} \sim 0.8\text{--}1R_{200\text{m}}$ in a cluster with high accretion rate, whereas R_{sp} is of about $1.5R_{200\text{m}}$ in a cluster with low accretion rate. Fong and Hun (2021) determined the galaxy cluster radius, which contains the splashback orbits of most of the galaxies, and which is equal to about $2\text{--}3R_{\text{sp}}$.

The authors of a number of studies search for and measure this radius in observed galaxy clusters (mostly distant ones with $z > 0.1$). The R_{sp} radii were measured using various methods: based on the surface density of galaxies (Adhikari et al. 2016; More et al. 2016; Baxter et al. 2017) or using the method of weak gravitational lensing (Umetsu and Diemer 2017; Chang et al 2018; Contigiani et al. 2019). In their simulations, Bucsh and White (2017) used the same algorithm for identifying galaxy clusters as the one employed for real observational data, and showed that the effect of the projection of background galaxies onto the cluster may distort the measured R_{sp} radius. A sample of galaxy clusters selected based not on the optical parameters but rather of the SZ signal, which better correlates with mass, also made it possible to measure the R_{sp} radii (Shin et al. 2019; Zúrcher and More 2019). Measuring the R_{sp} radius (the size of the dark-matter halo) in galaxy clusters using various methods is of great importance for the study of the large-scale structure of the Universe.

In this study we analyze observational manifestations of the splashback feature in a sample of groups and clusters of galaxies (based on SDSS data). Earlier, we found the “boundary” of 29 galaxy clusters clearly identified by the integrated distribution of the squared clustercentric distance of all cluster galaxies. We call this boundary the halo radius R_h (Kopylov and Kopylova 2015). This radius is usually greater than R_{200} and is measured from the projected profile, i.e., by the point of transition from the steep increase of the number of galaxies at the cluster center to its linear

decrease. We later identified this radius with the splashback radius R_{sp} reported the results for about 100 groups and clusters of galaxies (Kopylov and Kopylova 2015; Kopylova and Kopylov 2016, 2018, 2019). Kopylova and Kopylov (2018, 2019) showed that the distribution of early-type galaxies in clusters can be used to more precisely estimate the required radius. We analyzed the data for 40 systems to find the mean radius to be $R_{\text{sp}} = 1.54 \pm 0.06 R_{200}$ or $R_{\text{sp}} = 0.96 \pm 0.06 R_{200\text{m}}$ (given that $4R_{200} \approx 2.5R_{200\text{m}}$), which varies from 1.10 Mpc for the NGC 5627 group with $\sigma = 314 \text{ km s}^{-1}$ to 4.17 Mpc for the Coma cluster (A 1656) with $\sigma = 921 \text{ km s}^{-1}$.

In this study we increased the size of our sample to 157 groups and clusters of galaxies from the regions of Leo, Hercules, Ursa Major, Corona Borealis, and Bootes superclusters, from the region of A 1656/A1367, supercluster, as well as smaller superclusters and the field.

In our study we used the data from the SDSS (Sloan Digital Sky Survey, DRs 7, 8) and 2MASS XSC (2MASX, Two-Micron ALL-Sky Survey Extended Source Catalog) catalogs and from NED (NASA Extragalactic Database).

The paper has the following layout. Section 2 describes the sample of groups/clusters of galaxies and the procedure we use to determine the radii R_{sp} and R_c of the objects studied. Section 3 presents the construction of the dependences of the inferred radii on the basic parameters of groups and clusters of galaxies, which we determined in earlier studies. Section 4 summarizes the main results of this work. We use the following values of cosmological parameters: $\Omega_m = 0.3$, $\Omega_\Lambda = 0.7$, $H_0 = 70 \text{ km s}^{-1} \text{ Mpc}^{-1}$.

2. DESCRIPTION OF THE DATA AND THE TECHNIQUE FOR MEASURING THE RADII

Our sample consists of 157 groups and clusters from the regions of Leo ($N = 12$), Hercules ($N = 27$), Ursa Major ($N = 19$), Corona Borealis ($N = 7$), Bootes ($N = 13$), and other smaller superclusters and field regions ($N = 11$, $N = 20$), and groups of galaxies from the region

of A1656/A1367 supercluster ($N = 48$). The sample of galaxies in superclusters was compiled for measuring the peculiar velocities of their constituent galaxy clusters. In addition, we also analyzed the dependence between the dynamical mass within the virialized radius R_{200} and the K -band infrared luminosity (based on 2MASX data). X-ray radiation was recorded from all galaxy clusters except 21 groups of galaxies. We adopt their X-ray luminosities from catalogs of galaxy clusters based on ROSAT data (see the above papers for more detailed references). Our sample of groups and clusters of galaxies spans the maximum interval of line-of-sight velocities ranging from 200 to 1100 km s⁻¹ and have redshifts $0.01 < z < 0.10$.

For these groups and clusters we measured the heliocentric redshifts, line-of-sight velocity dispersions with cosmological correction $(1+z)^{-1}$ applied, the R_{200} radii, K -band luminosities $L_{K,200}$ ($M_K < -21^m$), dynamical masses M_{200} , and other parameters within the R_{200} radius (Kopylov and Kopy-

lova 2015; Kopylova and Kopylov 2016, 2017, 2018, 2019). The physical properties of the galaxy groups and clusters studied are listed in Columns (1)–(13) of Table 1.

The empirical cluster radius R_{200} can be predicted based on the dispersion of line-of-sight velocities provided that the cluster mass satisfies the condition $M(r) \propto r$. This radius can be estimated by the formula $R_{200} = \sqrt{3} \sigma / (10H(z))$ Mpc (Carlberg et al. 1997). In this case, if we assume that the cluster is virialized inside this radius, its mass can be found by the formula $M_{200} = 3G^{-1}R_{200}\sigma^2$, where σ is the one-dimensional dispersion of the line-of-sight velocities of galaxies located inside the R_{200} radius and G is the gravitational constant. Thus the cluster mass that we measure $M_{200} \propto \sigma^3$. The mass M_{200} contained in the spherical halo of radius R_{200} can also be measured directly based on the critical density, which depends on z : $M_{200} = \frac{4}{3}\pi R_{200}^3 \times 200\rho_c$.

Table 1. Dynamical parameters of groups and clusters of galaxies: (1)—the name of the cluster of galaxies; (2)—the heliocentric redshift; (3)—the line-of-sight velocity dispersion with cosmological correction $(1+z)^{-1}$ applied; (4)—the halo mass $\log M_{200}/M_\odot$; (5)—the K -luminosity $\log L_{K,200}/L_\odot$; (6)—the X-ray (0.1–2.4 keV) luminosity $\log L_X$ from X-ray catalogs of galaxy clusters based on ROSAT observations (we recomputed the luminosities using our inferred line-of-sight velocities of clusters and the adopted model); (7)—references to the X-ray luminosity; (8)—the R_{200} radius in Mpc; (9)—the R_{sp} radius in Mpc; (10)—the R_c radius in Mpc; (11)— R_{sp}/R_{200} ; (12)—the magnitude gap $\Delta M_{1,4}$ between the first and fourth brightest galaxies, and (13)—the concentration Σ_5 of galaxies brighter than $M_K = -23^m$ calculated by using the projected distance to the fifth galaxy closest to the center.

^a X-ray references: (1) Kopylova and Kopylov (2009), (2) Kopylova and Kopylov (2011), (3) Kopylova and Kopylov (2013), (4) Boöhringer et al. (2000), (5) Ebeling et al. (1998), (6) Kopylova and Kopylov (2016), (7) Kopylov and Kopylova (2007), (8) Kopylov and Kopylova (2012), (9) Kopylov and Kopylova (2010), (10) Kopylova and Kopylov (2017), (11) Boöhringer et al. (2004), (12) Mahdavi et al. (2000), (13) Ebeling et al. (2002), (14) Mulchaey et al. (2003), (15) Ledlow et al. (2003).

System	z_h	σ , km s ⁻¹	$\log M_{200}$, [M_\odot]	$\log L_{K,200}$, [L_\odot]	$\log L_X$, erg s ⁻¹	Ref ^a	R_{200} , Mpc	R_{sp} , Mpc	R_c , Mpc	R_{sp}/R_{200}	$\Delta M_{1,4}$	Σ_5 , Mpc ⁻²
(1)	(2)	(3)	(4)	(5)	(6)	(7)	(8)	(9)	(10)	(11)	(12)	(13)
HCG 42	0.012588	228	13.30	11.79	42.28	(6)	0.56	0.75	0.30	1.34	2.31	0.54
AWM 3	0.014878	269	13.52	11.68	<42.00	(12)	0.66	1.04	0.44	1.58	1.55	0.52
NGC 2563	0.015701	369	13.93	12.15	42.23	(6)	0.91	1.00	0.39	1.10	1.30	1.23
AWM 7	0.017344	698	14.77	12.62	43.98	(13)	1.71	1.97	1.08	1.15	2.28	2.07
NGC 0533	0.018411	404	14.05	12.25	42.84	(6)	0.99	1.40	0.57	1.41	3.24	0.32
NGC 0741	0.018416	368	13.93	12.10	42.60	(6)	0.90	0.98	0.39	1.09	2.98	0.66

Table 1. (Continued)

System	z_h	σ , km s ⁻¹	$\log M_{200}$, [M_\odot]	$\log L_{K, 200}$, [L_\odot]	$\log L_X$, erg s ⁻¹	Ref ^a	R_{200} , Mpc	R_{sp} , Mpc	R_c , Mpc	R_{sp}/R_{200}	$\Delta M_{1,4}$	Σ_5 , Mpc ⁻²
(1)	(2)	(3)	(4)	(5)	(6)	(7)	(8)	(9)	(10)	(11)	(12)	(13)
NGC 0080	0.019098	296	13.64	12.29	42.84	(6)	0.73	0.79	0.37	1.08	1.31	1.48
MKW 04	0.020208	515	14.37	12.41	43.15	(11)	1.26	1.53	0.78	1.21	1.84	1.72
NGC 3022	0.020959	276	13.56	11.97	<42.30	(12)	0.68	1.14	0.50	1.68	1.50	1.20
A 1367	0.021743	749	14.86	12.89	43.91	(5)	1.84	2.74	1.38	1.49	0.89	2.25
NGC 2783	0.022151	346	13.85	12.04	42.00	(14)	0.85	1.02	0.59	1.20	3.04	0.60
UGC 07115	0.022199	334	13.81	12.12	42.60	(6)	0.82	1.06	0.66	1.29	1.79	0.78
UGC 02005	0.022342	352	13.88	12.05	42.60	(6)	0.86	1.12	0.59	1.30	1.43	0.72
IC 5357	0.022436	381	13.98	12.08	42.70	(6)	0.93	1.02	0.57	1.10	0.96	1.00
NGC 1016	0.022581	322	13.76	12.28	<42.30	(12)	0.79	1.10	0.40	1.39	2.01	1.11
NGC 3158	0.022630	375	13.95	12.25	42.48	(6)	0.92	1.24	0.32	1.35	2.01	1.67
NGC 0070	0.022645	415	14.09	12.30	42.95	(6)	1.02	1.15	0.62	1.13	0.31	2.72
AWM 2	0.022761	293	13.63	11.97	–		0.72	0.78	0.42	1.08	2.18	0.64
NGC 5171	0.023000	371	13.94	12.18	43.00	(6)	0.91	1.47	0.58	1.62	0.84	1.63
NGC 2832	0.023044	331	13.79	12.25	43.00	(6)	0.81	1.25	0.63	1.54	2.34	1.32
A 1656	0.023250	921	15.13	13.22	44.57	(5)	2.26	4.17	2.00	1.84	1.78	2.02
NGC 5129	0.023402	290	13.62	12.11	42.95	(6)	0.71	1.36	0.55	1.92	3.01	0.84
MCG-0129015	0.023813	334	13.81	12.02	42.64	(12)	0.82	1.56	0.60	1.90	1.72	0.66
NGC 7436B	0.024720	383	13.98	12.24	<42.00	(12)	0.94	1.08	0.48	1.15	1.84	1.53
NGC 5306	0.024732	305	13.68	12.06	42.70	(6)	0.75	1.30	0.58	1.73	3.22	0.78
NGC 5223	0.024834	271	13.53	12.19	42.78	(6)	0.66	0.97	0.36	1.47	2.09	1.20
MKW 05	0.024858	288	13.61	11.84	–		0.70	0.88	0.26	1.26	2.12	0.46
NGC 4325	0.025386	271	13.53	11.79	42.71	(6)	0.66	0.84	0.41	1.27	2.04	0.40
IC 01867	0.026023	318	13.74	12.10	<42.30	(6)	0.78	1.16	0.58	1.49	1.97	0.93
NGC 7237	0.026102	376	13.96	12.20	42.75	(6)	0.92	1.58	0.60	1.72	1.26	1.45
IC 02476	0.026198	243	13.38	11.88	<42.30	(12)	0.59	0.96	0.32	1.63	2.12	0.71
NGC 5627	0.026682	314	13.72	12.14	42.30	(6)	0.77	1.10	0.53	1.43	2.49	0.85
MKW 08	0.026906	450	14.19	12.50	43.48	(3)	1.10	1.73	0.85	1.57	0.63	2.00
UGC 05088	0.027622	247	13.41	11.72	42.30	(3)	0.60	0.90	0.41	1.50	1.79	0.43
MKW 04s	0.027928	423	14.11	12.27	43.04	(5)	1.03	1.53	0.78	1.48	2.17	1.28
AWM 1	0.028652	402	14.05	12.37	<42.30	(12)	0.98	1.15	0.62	1.17	1.14	1.61
NGC 2795	0.028992	431	14.14	12.38	42.70	(3)	1.04	1.32	0.62	1.27	1.94	1.00
NGC 6338	0.029342	552	14.46	12.45	43.40	(3)	1.35	2.12	0.50	1.57	2.00	1.65
NGC 3119	0.029657	355	13.88	12.19	42.60	(6)	0.87	1.20	0.60	1.38	2.50	1.61
NGC 5758	0.029923	291	13.62	12.09	42.84	(6)	0.71	1.09	0.50	1.54	1.11	1.49
A 2199	0.030458	746	14.85	13.01	44.31	(3)	1.82	3.56	1.42	1.96	0.70	2.36
A 2197	0.030477	547	14.45	12.85	43.08	(3)	1.34	1.80	0.92	1.34	1.54	–
NGC 6107	0.031093	546	14.44	12.55	43.23	(3)	1.33	1.90	1.03	1.43	0.45	1.32
NGC 6159	0.031320	266	13.51	11.81	42.78	(3)	0.65	0.89	0.45	1.37	2.60	0.48
AWM 4	0.031827	380	13.97	12.04	43.36	(3)	0.93	1.34	0.57	1.44	3.13	0.61
A 0999	0.031866	248	13.41	12.05	42.48	(2)	0.60	1.11	0.53	1.85	2.18	1.18
UGC 04991	0.031958	515	14.37	12.37	42.60	(3)	1.26	1.72	0.65	1.36	1.25	1.73
A 2162	0.032147	346	13.85	12.17	42.60	(3)	0.84	1.12	0.63	1.33	1.89	1.08
A 1177	0.032159	337	13.81	12.09	43.04	(2)	0.82	1.14	0.55	1.39	2.33	0.85
A 1016	0.032178	267	13.51	12.09	–		0.65	1.02	0.35	1.57	1.76	1.11
A 1314	0.032443	494	14.31	12.49	43.11	(2)	1.18	1.90	0.55	1.61	0.97	1.46
A 1185	0.032734	676	14.72	12.84	43.18	(2)	1.69	2.19	0.84	1.30	1.06	2.28
A 1257	0.034588	242	13.38	11.91	–		0.58	0.99	0.40	1.71	1.08	1.28
A 2063	0.034664	753	14.86	12.79	44.01	(3)	1.83	2.61	1.10	1.43	0.90	2.00
A 2052	0.034726	623	14.61	12.70	44.11	(3)	1.52	2.12	0.87	1.39	1.28	1.80
AWM 5	0.035043	517	14.37	12.67	43.45	(3)	1.24	1.70	0.89	1.37	1.93	1.00
A 1228A	0.035055	216	13.23	12.18	–		0.57	1.00	0.47	1.75	0.73	1.36

Table 1. (Continued)

System	z_h	σ , km s ⁻¹	$\log M_{200}$, [M_\odot]	$\log L_{K, 200}$, [L_\odot]	$\log L_X$, erg s ⁻¹	Ref ^a	R_{200} , Mpc	R_{sp} , Mpc	R_c , Mpc	R_{sp}/R_{200}	$\Delta M_{1,4}$	Σ_5 , Mpc ⁻²
(1)	(2)	(3)	(4)	(5)	(6)	(7)	(8)	(9)	(10)	(11)	(12)	(13)
RXC J1057.7+3739	0.035208	297	13.65	11.93	42.48	(2)	0.72	0.97	0.46	1.35	1.69	1.08
VV 196	0.035289	412	14.08	12.12	42.85	(3)	1.00	1.17	0.71	1.17	1.09	2.48
A 2147	0.036179	853	15.02	13.11	44.20	(3)	2.08	3.47	1.49	1.67	0.56	1.82
A 2151	0.036378	734	14.83	13.08	43.65	(3)	1.79	2.10	0.55	1.17	0.63	1.68
NGC 5098	0.036812	445	14.18	12.46	43.11	(3)	1.08	1.73	0.71	1.60	0.92	1.93
RXC J1511.5+0145	0.038990	374	13.95	12.10	42.95	(3)	0.91	1.12	0.63	1.23	1.65	0.80
A 1139	0.039327	459	14.21	12.57	43.18	(2)	1.12	1.64	0.71	1.46	0.84	1.79
RBS 858	0.039586	445	14.18	12.39	43.11	(2)	1.08	1.64	0.84	1.52	1.81	1.04
A 2107	0.041335	581	14.52	12.69	43.77	(3)	1.41	2.17	0.63	1.54	1.40	1.61
A 1228B	0.042892	347	13.85	12.25	42.78	(2)	0.84	1.28	0.50	1.52	2.70	0.70
A 1983	0.044803	460	14.22	12.70	43.41	(3)	1.12	1.34	0.78	1.20	0.62	2.24
MKW 03s	0.044953	608	14.58	12.67	44.15	(3)	1.47	1.95	0.76	1.33	0.66	1.74
A 0957	0.045026	689	14.74	12.70	43.61	(3)	1.67	1.79	0.99	1.07	2.23	1.93
A 2040	0.045242	589	14.54	12.82	43.26	(3)	1.43	2.20	0.84	1.54	0.58	2.62
RXC J1010.3+5430	0.045877	384	13.98	12.36	42.30	(1)	0.93	1.20	0.81	1.29	1.92	0.73
A 1100	0.046463	402	14.04	12.31	42.78	(3)	0.97	1.22	0.55	1.26	1.74	1.77
RXC J1722.2+3042	0.046580	524	14.39	12.56	42.70	(3)	1.27	1.64	0.67	1.29	1.78	1.40
RXC J0748.2+1833	0.046602	454	14.20	12.60	43.15	(3)	1.09	1.28	0.71	1.17	1.73	2.24
SHK 352	0.049521	532	14.41	12.60	43.43	(4)	1.29	2.17	0.74	1.68	0.64	2.22
A 0671	0.049802	805	14.95	12.89	43.66	(6)	1.95	1.97	0.84	1.01	1.68	2.26
Sh 166	0.050043	323	13.76	12.17	–		0.78	1.38	0.56	1.77	1.22	1.52
Z 2844	0.050489	401	14.04	12.39	43.46	(5)	0.97	1.48	0.63	1.52	2.05	1.30
A 0757	0.051319	368	13.92	12.43	43.66	(6)	0.89	1.79	0.77	2.01	0.46	1.85
A 1291A	0.051349	391	14.00	12.17	43.34	(1)	0.94	1.48	0.55	1.57	1.32	0.86
A 1377	0.051807	632	14.63	12.77	43.45	(1)	1.53	2.05	0.63	1.34	0.71	2.27
A 1461	0.053962	317	13.73	11.92	–		0.76	1.13	0.49	1.49	1.22	1.15
RXC J1022.2+3831	0.054163	551	14.45	12.65	43.26	(6)	1.33	1.57	0.84	1.18	0.71	1.45
RXC J0844.9+4258	0.054858	320	13.74	12.16	42.90	(10)	0.77	1.30	0.63	1.69	2.25	0.86
RXC J1122.2+6713	0.055119	237	13.34	11.79	42.78	(1)	0.57	1.07	0.42	1.88	2.42	0.68
A 1318	0.056419	394	14.01	12.48	42.60	(1)	0.95	1.26	0.68	1.33	1.19	1.40
RXC J1654.4+2334	0.057075	383	13.98	12.27	43.26	(10)	0.92	1.26	0.77	1.37	1.70	1.30
A 1291B	0.057161	396	14.02	12.07	–		0.95	1.05	0.50	1.11	1.34	1.04
A 2169	0.057656	502	14.33	12.46	43.36	(5)	1.21	1.45	0.63	1.20	0.44	1.26
A 1991	0.058463	554	14.46	12.81	43.85	(6)	1.33	1.49	0.95	1.12	0.99	1.59
RXC J0746.7+3059	0.058482	317	13.73	12.21	43.20	(4)	0.76	0.90	0.56	1.18	0.63	2.20
A 1383	0.059583	464	14.23	12.58	43.11	(1)	1.12	1.67	0.95	1.49	0.90	1.68
A 1507	0.059967	432	14.13	12.42	42.85	(1)	1.02	1.53	0.63	1.50	1.19	1.08
A 0602	0.060551	560	14.47	12.64	43.76	(6)	1.35	1.90	0.92	1.41	0.31	1.51
RXC J1224.8+3156	0.060664	454	14.20	12.40	43.18	(4)	1.09	1.73	0.95	1.59	0.70	1.52
Anon 4	0.061053	397	14.02	12.39	–		0.96	1.52	0.64	1.58	1.47	1.64
A 1452	0.061649	408	14.06	12.28	–		0.98	1.10	0.59	1.12	1.21	1.28
A 1781	0.062264	362	13.90	12.44	–		0.87	1.56	0.65	1.79	1.35	1.28
A 1795	0.062444	775	14.89	12.95	44.76	(6)	1.86	3.06	1.34	1.64	1.39	2.09
A 1275	0.062750	348	13.85	12.29	43.34	(6)	0.84	1.20	0.67	1.43	1.58	1.11
A 1003	0.062763	575	14.50	12.49	43.00	(1)	1.38	1.66	0.77	1.20	1.32	1.36
RXC J1351.7+4622	0.062915	528	14.40	12.60	43.08	(4)	1.29	1.70	0.92	1.32	2.01	0.90
A 1831A	0.062942	480	14.27	12.48	–		1.15	1.43	0.69	1.24	1.12	1.57
A 1825	0.063274	633	14.63	12.56	43.04	(6)	1.52	1.38	0.55	0.91	0.95	1.70
A 1668	0.063699	635	14.63	12.72	43.91	(5)	1.52	1.82	0.95	1.20	1.42	1.85
A 1436	0.064960	700	14.76	12.83	43.72	(1)	1.68	1.82	1.41	1.08	0.37	1.76
A 2149	0.065253	361	13.90	12.46	43.62	(10)	0.87	1.28	0.63	1.47	2.23	1.57

Table 1. (Continued)

System	z_h	σ , km s ⁻¹	$\log M_{200}$, [M_\odot]	$\log L_{K, 200}$, [L_\odot]	$\log L_X$, erg s ⁻¹	Ref ^a	R_{200} , Mpc	R_{sp} , Mpc	R_c , Mpc	R_{sp}/R_{200}	$\Delta M_{1,4}$	Σ_5 , Mpc ⁻²
(1)	(2)	(3)	(4)	(5)	(6)	(7)	(8)	(9)	(10)	(11)	(12)	(13)
A 1775A	0.065591	324	13.76	12.31	–		0.78	1.64	0.45	2.10	1.07	1.56
A 2124	0.065722	736	14.83	12.83	43.84	(6)	1.77	2.21	0.92	1.25	1.73	1.84
A 2079	0.065746	618	14.60	12.95	43.57	(6)	1.48	2.12	0.95	1.43	0.97	1.26
RXC J1206.6+2215	0.065786	269	13.52	12.08	43.15	(10)	0.65	1.22	0.60	1.88	2.41	1.18
A 2092	0.066564	486	14.29	12.52	43.60	(6)	1.17	2.05	0.76	1.75	0.80	2.17
Anon 3	0.067960	380	13.96	12.29	–		0.91	1.26	0.50	1.38	1.25	1.52
A 1035A	0.067997	563	14.48	12.63	42.85	(7)	1.35	1.79	0.90	1.33	0.35	1.72
A 1569A	0.068759	484	14.26	12.44	43.30	(8)	1.16	1.50	0.60	1.29	0.82	2.82
A 1371	0.068891	552	14.45	12.67	43.53	(4)	1.32	2.12	0.90	1.61	0.86	1.91
A 1066	0.068917	768	14.88	12.98	43.82	(4)	1.84	3.03	1.26	1.65	0.95	1.63
A 1270	0.068939	524	14.38	12.68	42.78	(1)	1.26	1.41	0.95	1.12	0.34	1.92
A 1534	0.069848	322	13.75	12.41	–		0.77	1.40	0.57	1.82	1.96	1.26
Anon 1	0.069884	608	14.58	12.70	43.54	(1)	1.47	1.76	1.14	1.20	1.21	1.79
A 1767	0.070326	816	14.96	13.03	44.10	(5)	1.95	2.55	1.10	1.31	1.50	2.05
Z 6718	0.071374	550	14.45	12.54	43.80	(5)	1.32	2.00	0.87	1.52	1.04	1.81
A 1904	0.071708	771	14.89	13.07	43.67	(15)	1.84	2.02	1.12	1.10	1.10	2.21
RXC J1054.2+5450A	0.071886	507	14.34	12.68	43.72	(1)	1.21	1.52	0.93	1.26	0.29	2.05
A 1589	0.071955	778	14.90	13.06	44.23	(8)	1.86	3.11	1.55	1.67	0.96	1.74
A 2065	0.072211	1104	15.35	13.31	44.40	(6)	2.64	3.36	1.67	1.27	0.54	2.82
A 1024	0.073296	578	14.51	12.60	43.40	(4)	1.38	1.83	0.59	1.33	1.43	2.58
A 2089	0.073546	531	14.40	12.66	43.15	(15)	1.27	1.48	0.91	1.16	1.44	1.30
A 2064	0.073689	633	14.63	12.66	43.86	(4)	1.51	1.67	1.00	1.11	1.96	1.79
J1051.8+5523B	0.073762	420	14.09	12.49	–		1.00	1.22	0.71	1.22	1.75	1.53
A 1238	0.074111	541	14.42	12.78	43.41	(6)	1.29	2.12	0.90	1.64	1.03	2.66
A 1775B	0.075138	581	14.52	12.78	44.20	(6)	1.39	1.78	0.81	1.28	1.95	1.65
A 1203	0.075307	416	14.08	12.64	–		0.99	1.45	0.67	1.46	1.32	1.41
A 1800	0.075321	705	14.77	12.91	44.19	(6)	1.68	2.28	1.24	1.36	2.02	1.86
A 1190	0.075334	670	14.70	12.91	43.88	(5)	1.60	1.95	0.89	1.22	1.12	1.64
A 1831B	0.075481	952	15.16	12.97	44.18	(9)	2.27	2.85	1.64	1.26	1.17	2.19
A 1424	0.075900	632	14.63	12.82	43.71	(4)	1.51	1.82	1.12	1.20	1.33	2.02
A 1205	0.076103	787	14.91	12.98	44.02	(4)	1.88	2.26	1.34	1.20	1.76	1.74
A 1516	0.076166	660	14.68	12.87	–		1.58	1.82	1.34	1.15	1.53	2.23
A 1173	0.076193	516	14.36	12.61	43.70	(5)	1.23	1.97	0.67	1.60	1.21	1.89
J1350.2+2913	0.076439	359	13.89	12.40	–		0.86	1.30	0.41	1.51	0.89	1.83
Z 4905	0.076817	568	14.49	12.67	43.79	(5)	1.36	2.00	1.00	1.47	1.73	1.73
Z 5029	0.077360	912	15.10	13.15	44.43	(5)	2.18	2.55	1.48	1.17	0.92	2.58
A 1773	0.077425	832	14.98	12.98	43.89	(5)	1.98	2.43	1.10	1.23	1.20	2.54
A 2061	0.077746	712	14.78	13.12	44.31	(6)	1.70	1.95	0.97	1.15	1.15	1.88
A 2029	0.077812	1046	15.28	13.37	44.89	(6)	2.50	4.24	1.53	1.70	2.35	2.21
A 1780	0.077855	474	14.25	12.70	–		1.13	1.82	0.78	1.61	0.90	1.76
A 1035B	0.078276	613	14.59	12.58	43.30	(7)	1.46	1.61	0.84	1.10	1.47	2.07
A 1898	0.078525	434	14.13	12.47	43.04	(6)	1.04	1.90	0.81	1.83	0.50	–
A 1809	0.079290	729	14.81	12.99	43.91	(5)	1.74	2.47	1.10	1.42	1.45	1.65
A 1569B	0.079331	493	14.30	12.46	–		1.18	1.69	0.67	1.43	1.71	1.88
A 2019	0.081176	345	13.83	12.27	43.18	(6)	0.82	1.22	0.59	1.49	1.78	1.34
A 1750	0.085934	747	14.84	13.15	44.32	(11)	1.78	2.30	1.23	1.29	1.24	2.00
A 2245	0.087950	1037	15.27	13.25	43.67	(5)	2.46	2.93	1.10	1.19	1.45	1.99
A 2142	0.090135	963	15.17	13.42	45.02	(6)	2.28	4.12	1.52	1.81	0.83	1.83
A 2244	0.098993	1049	15.28	13.18	44.68	(5)	2.48	3.19	1.48	1.28	1.85	1.87

We first estimate the average line-of-sight velocity of the cluster, cz , and its dispersion σ ,

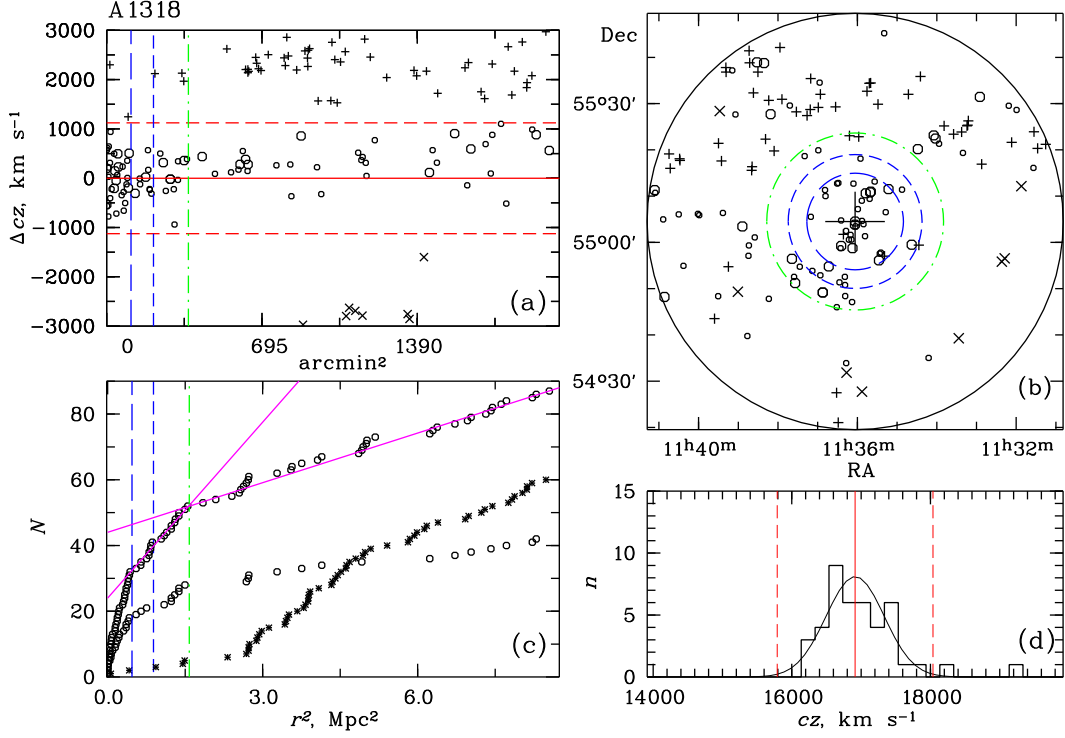


Figure 1. Distribution of galaxies in the A 1318 cluster. Panel (a) shows the deviation of line-of-sight velocities of galaxies from the mean line-of-sight velocity of the cluster inferred from the galaxies located within the R_{200} radius. The red horizontal dashed lines correspond to $\pm 2.7\sigma$ deviations. The vertical lines show the R_{200} (short dashes), R_A (long dashes), and R_{sp} (dashed-and-dotted line) radii. Larger circles, plus symbols, and crosses indicate galaxies brighter than $M_K^* + 1 = -24^m$, field galaxies, respectively. Panel (b) shows the sky distribution of galaxies from panel (a) in the equatorial system (the same designations are used). The circles outline regions with the radii R_{200} (short dashes), R_c (long dashes), and R_{sp} (dashed-and-dotted). The region under study is limited to the circle of radius $3.5R_{200}$ (the black solid line). The large cross indicates the cluster center. Panel (c) shows the integrated distributions of the total number of galaxies (the top curve) and early-type galaxies brighter than $M_K < -21^m.5$ (the bottom curve) as a function of the squared distance from the center of the group. Circles correspond to galaxies shown by circles in panel (a) and asterisks, to foreground and background galaxies. The solid magenta lines characterize the behavior of the distribution of galaxies inside and beyond the R_{sp} radius. Panel (d) shows the distribution of line-of-sight velocities of all galaxies inside the R_{200} radius (the solid line for cluster members shows the Gaussian corresponding to the dispersion of line-of-sight velocities). The solid vertical red line indicates the average line-of-sight velocity of the cluster and the dashed red lines correspond to $\pm 2.7\sigma$ deviations.

which we then use to estimate the R_{200} radius. We then determine the number of galaxies inside this radius and again compute the average line-of-sight velocity of the cluster, cz , its dispersion σ , and infer from it the radius R_{200} , etc. We thus move from the cluster center to iteratively determine the dispersion of line-of-sight velocities of galaxies and other cluster parameters within the given radius. We considered galaxies with relative velocities greater than 2.7σ to be field objects (e.g., Mamon et al. 2004), selection criteria usually vary from 2.5σ to 3.0σ .

To determine the radius R_{sp} , it is important to select the closest neighborhoods of groups/clusters of galaxies. To this end, we use a set of figures that characterize in detail the structure and kinematics of clusters of galaxies, namely:

- (a) deviation of the line-of-sight velocities of cluster member galaxies and galaxies classified as field objects from the mean line-of-sight velocity of the cluster or group as a function of the squared radius (cluster-centric distance);

- (b) sky positions of galaxies in equatorial coordinates;
- (c) integrated distribution of the number of all galaxies as a function of the squared radius;
- (d) histogram of the distribution of line-of-sight velocities of all galaxies inside the R_{200} radius.

As an example, we show in Fig. 1–4 such plots for A 1318, A 1377, A 1767 and Zw 2844 clusters, respectively.

Of special interest is the the projected cluster profile, i.e., the integrated distribution of the number of galaxies as a function of the squared clustercentric distance as shown in panels (c) of the analyzed plots (see Figs. 1–4). This distribution allows us to visually identify the dense core of the group/cluster, its more tenuous envelope, and the outer region, where the distribution becomes linear (shown by the solid magenta line in panels (c) of Figs. 1–4) in the adopted coordinates, i.e., the distribution of galaxies appears, on the average, uniform (Kopylov and Kopylova 2015). The dashed and dashed-and-dotted lines in panels (b) of Figs. 1–4 show the radius of the virialized region R_{200} and the radius R_{sp} beyond which the distribution of the number of cluster members becomes linear, respectively. We also outlined with the long-dashed curve the central part of the cluster with radius R_c where the main sharp increase of the number of galaxies is observed. Panels (c) (Figs. 1–4) show the distribution of early-type galaxies brighter than $M_K = -21^m5$, which was used to refine these radii. Such galaxies are usually located in central virialized regions of groups/clusters of galaxies. Our inferred splashback radius R_{sp} (Adhikari et al. 2014; Diemer and Kravtsov 2014) is the mean radius of the apocenters of the orbits of galaxies that have moved out of the central region of the galaxy cluster. That is, the inferred radius R_{sp} separates most of the galaxies that fall for the first time onto the cluster, from the galaxies from the galaxies that already belong to the cluster. We found for the entire sample $\langle R_{\text{sp}} \rangle = 1.67 \pm 0.05$ Mpc with a total spread 0.75–4.24, $\langle R_c \rangle = 0.78 \pm 0.03$ with a total spread of 0.30–2.00, $\langle R_{\text{sp}}/R_{200} \rangle = 1.40 \pm 0.02$ or $\langle R_{\text{sp}}/R_{200\text{m}} \rangle = 0.88 \pm 0.02$ (for $4R_{200c} \approx 2.5R_{200\text{m}}$), $\langle R_{\text{sp}}/R_c \rangle =$

2.19 ± 0.04 , $\langle R_{200c}/R_c \rangle = 1.58 \pm 0.02$. The range of R_{sp}/R_{200} ratios for our sample lies in the 0.91–1.96 interval and approximately agrees with the results of simulations, 1.28–2.4 (More et al. 2015).

Table 1 lists the measured R_{sp} and R_c radii and other physical properties of the groups and clusters of galaxies studied.

3. RESULTS

3.1. Dependences of radius R_{sp} on L_X and M_{200}

By definition $R_{\text{sp}} > R_{200}$ except for the cases where overestimated dispersion of line-of-sight velocities is observed in the cluster inside R_{200} —this value can (like in our case) affect the inferred R_{200} radius. Such clusters of galaxies (e.g., A 1825) usually show non-Gaussian distribution of line-of-sight velocities inside R_{200} .

We studied how the R_{sp} and R_c radii vary as a function of the properties of groups/clusters of galaxies. Fig. 5 shows the dependence of $\log R_{\text{sp}}$ on X-ray luminosity $\log L_X$, and, for comparison, a similar relation for the $\log R_{200}$ radius. The reported relations (straight lines) are averages of direct and inverse regressions with independent variables swapped. The dashed lines show the 1σ deviations from this regression. Note that the mean-square deviation for the dependence of radius R_{sp} is somewhat smaller than for radius R_{200} . The filled circles show merging groups/clusters of galaxies with bimodal distribution of line-of-sight velocities inside R_{200} . Note that the positions of these structures on common relations do not differ from those of groups/clusters of galaxies with Gaussian distribution of line-of-sight velocities. Our sample also contains the second group of galaxies with no measured X-ray luminosities. These are usually groups of galaxies with $\sigma \leq 400$ km s⁻¹. Table 2 lists the parameters of our derived relations—their slopes, intercepts, and scatters. The splashback radii of groups/clusters that we inferred from observed profiles yield the following relations:

$$R_{\text{sp}} \propto L_X^{0.24 \pm 0.03}, R_{\text{sp}} \propto (M_{200}/M_{\odot})^{0.32 \pm 0.02},$$

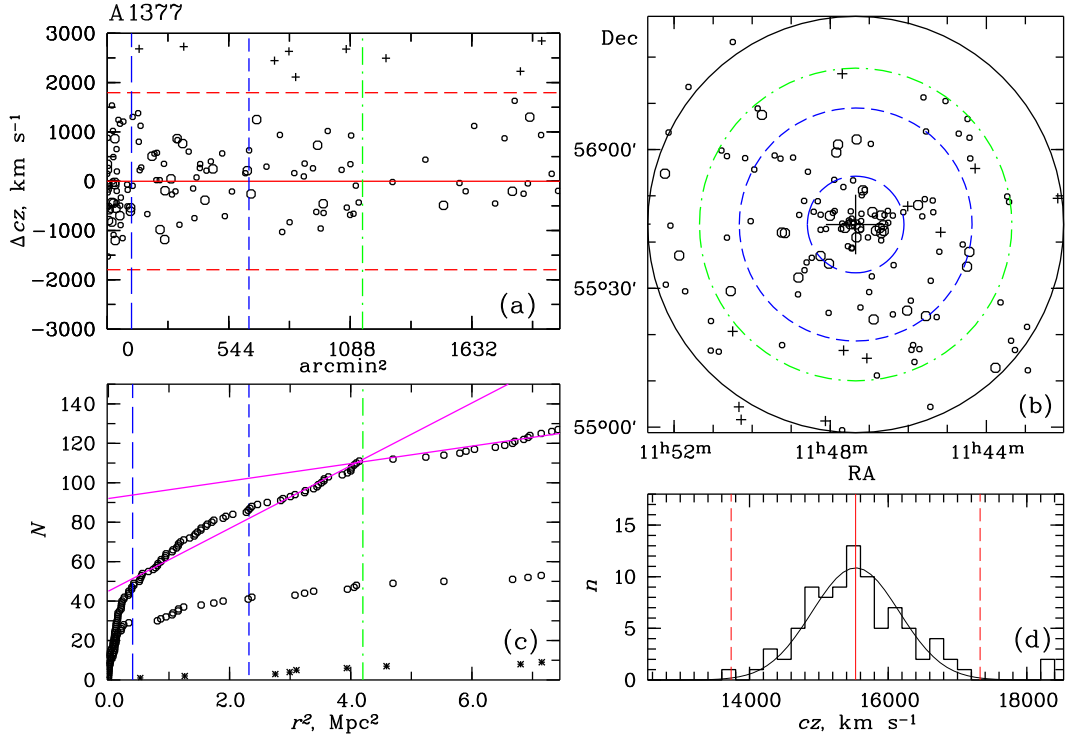


Figure 2. Distribution of galaxies in the A 1377 cluster. Designations are the same as in Fig. 1.

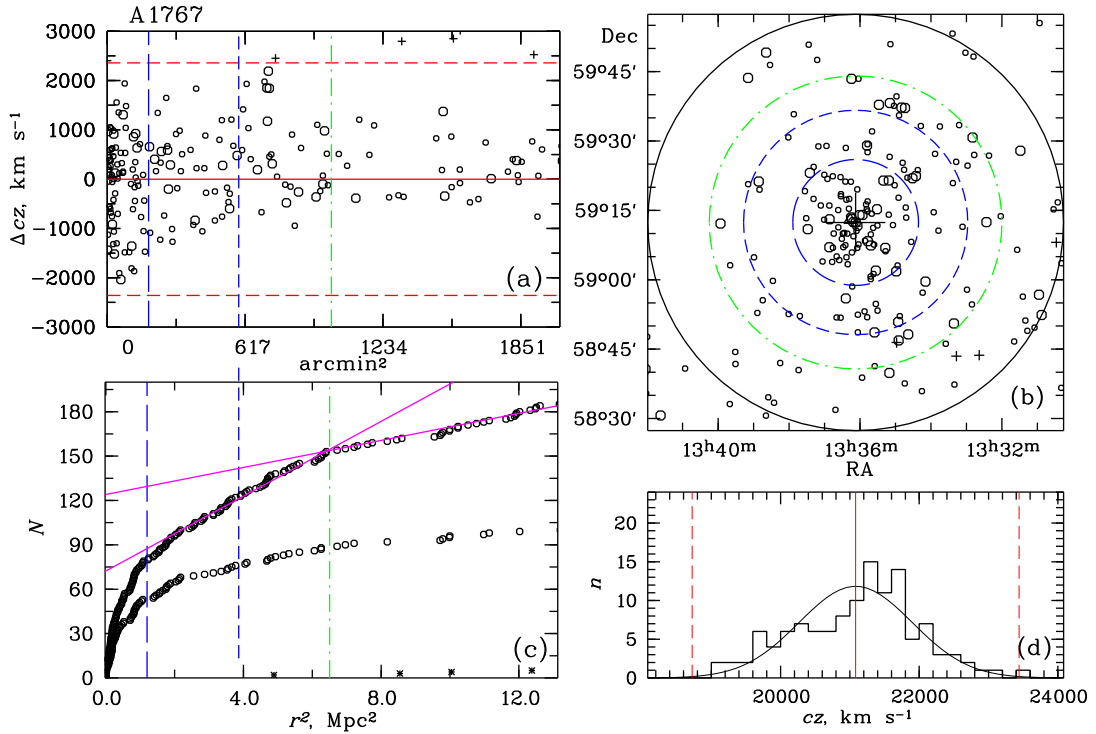


Figure 3. Distribution of galaxies in the A 1767 cluster. Designations are the same as in Fig. 1.

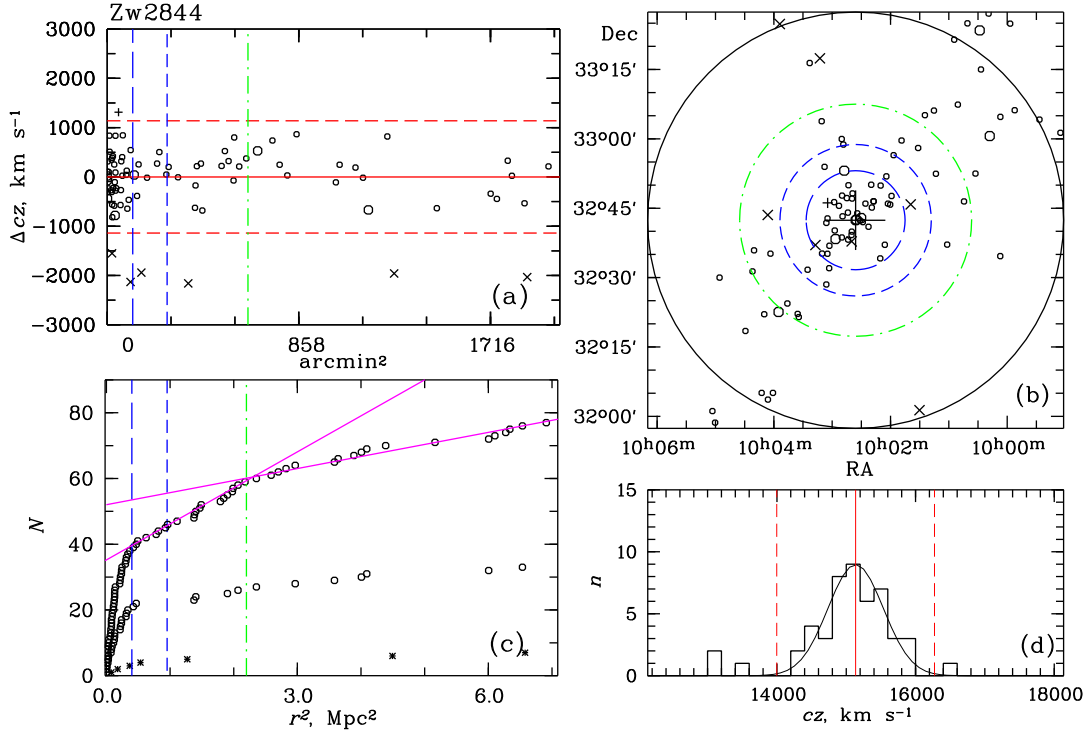


Figure 4. Distribution of galaxies in the Zw 2844 cluster. Designations are the same as in Fig. 1.

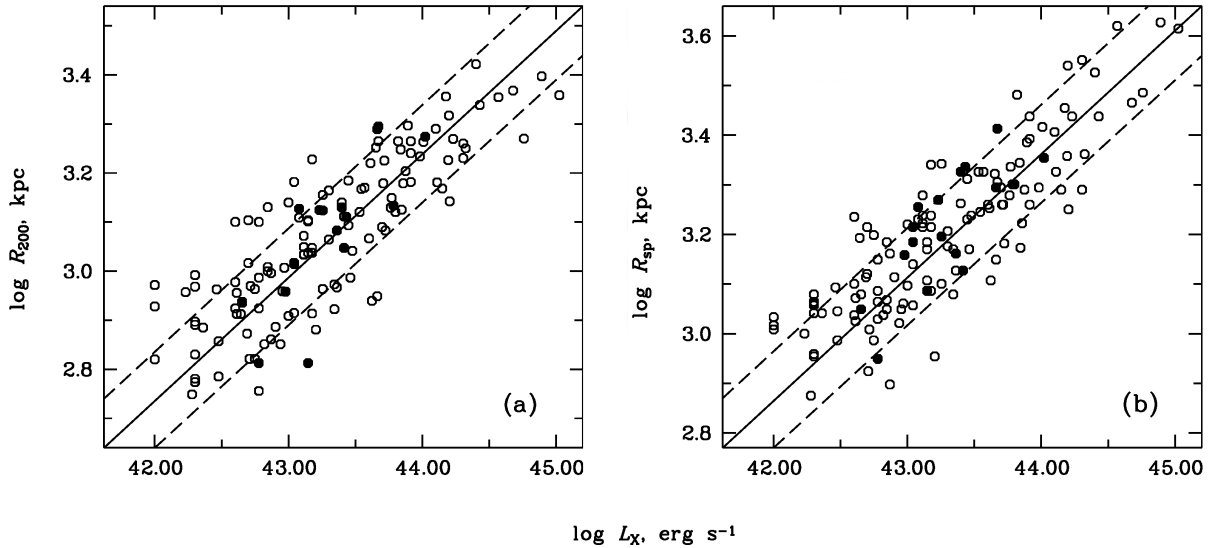


Figure 5. Dependence of radius R_{200} (a) and radius R_{sp} (b) on the 0.1–2.4 keV X-ray luminosity. The solid lines correspond to regression relations $R_{\text{sp}} \propto L_X^{0.24 \pm 0.03}$ and $R_{200} \propto L_X^{0.25 \pm 0.04}$. The dashed lines show the 1σ -deviations from these relations. The filled circles show groups and clusters with bimodal distribution of line-of-sight velocities.

Table 2. Examples of relations

Relation	Slope	Normalization	Scatter
$\log R_{\text{sp}} - \log L_X$	0.24 ± 0.03	-7.39 ± 0.33	0.092
$\log R_{200} - \log L_X$	0.25 ± 0.04	-7.60 ± 0.34	0.097
$\log R_c - \log L_X$	0.26 ± 0.04	-8.45 ± 0.37	0.110
$\log R_{\text{sp}} - \log(M_{200}/M_\odot)$	0.32 ± 0.02	-1.42 ± 0.13	0.066
$\log R_c - \log(M_{200}/M_\odot)$	0.35 ± 0.03	-2.08 ± 0.17	0.086
$\log R_{\text{sp}} - \log(L_K/L_\odot)$	0.42 ± 0.03	-2.00 ± 0.17	0.074
$\log R_{200} - \log(L_K/L_\odot)$	0.41 ± 0.02	-2.10 ± 0.12	0.052
$\log R_c - \log(L_K/L_\odot)$	0.44 ± 0.03	-2.66 ± 0.19	0.088
$\log R_{\text{sp}} - \log R_{200}$	1.00 ± 0.04	0.17 ± 0.11	0.064
$\log R_{\text{sp}} - \log R_c$	0.95 ± 0.05	0.46 ± 0.14	0.088
$\log R_{\text{sp}} - \log \Sigma_5$	0.31 ± 0.06	2.71 ± 0.17	0.158
$\log R_{\text{sp}} - \Delta M_{1,4}$	-0.08 ± 0.02	3.31 ± 0.03	0.147

$$R_{\text{sp}} \propto (L_K/L_\odot)^{0.42 \pm 0.03}.$$

The dependence on L_K luminosity (which characterizes galaxies) is almost twice steeper than the dependence on L_X luminosity (which characterizes gas). The dependences of the radius of the radius $\log R_A$ of the central part of the cluster are, on the average, steeper by 5% than the corresponding dependences for the $\log R_{\text{sp}}$ radius. The smallest scatter is observed for the dependence $\log R_{\text{sp}}$ on $\log(M_{200}/M_\odot)$. We do not give the dependence between $\log R_{200}$ and $\log M_{200}/M_\odot$ in Table 2 because the two variables are dependent.

3.2. Dependences of radius R_{sp} on Σ_5 and $\Delta M_{1,4}$

We measured the concentration of galaxies in groups and clusters as the internal density of galaxies, Σ_5 , computed from the distance to the fifth nearest galaxy brighter than $M_K = -23^m3$. The measured concentrations for a significant part of groups of galaxies were published by (Kopylova and Kopylov 2017). The above paper also provides the measured K - and r -band magnitude gap $\Delta M_{1,4}$ between the brightest and fourth brightest galaxies within the $0.5 R_{200}$ radius. In the cases where the $\Delta M_{1,4} \geq 2.5$ condition is fulfilled dynamically “old” groups with masses $M_{200} < 1.43 \times 10^{14} M_\odot$ can be found (Kopylova

and Kopylov 2017). Fig. 6 shows the dependences of radius R_{sp} on the concentration of galaxies (Fig. 6a) and on the $\Delta M_{1,4}$ magnitude gap (Fig. 6b). The filled circles show groups of galaxies with $\sigma \leq 400 \text{ km s}^{-1}$. The relation (the straight line) shown in Fig. 6a is the average of direct and inverse regressions with independent variable swapped, $R_{\text{sp}} \propto \Sigma_5^{0.31}$. The dashed lines show the 1σ deviations from this relation. In our earlier paper (Kopylova and Kopylov 2017) we showed that the concentration of galaxies in groups and clusters correlates with richness, X-ray luminosity, mass and the R_{sp} radius. An analysis of Fig. 6b shows that $\log R_{\text{sp}}$ depends slightly on $\Delta M_{1,4}$ separately for groups and clusters of galaxies. The combined sample yields $R_{\text{sp}} \propto 10^{-0.081 \Delta M_{1,4}}$, i.e., the greater $\Delta M_{1,4}$, the smaller is the R_{sp} radius for groups of galaxies. We already showed (Kopylova and Kopylov 2017) that in the $\Delta M_{1,4} - \Sigma_5$ diagram clusters of galaxies are located in the region of large concentrations of galaxies and small $\Delta M_{1,4}$, i.e., in the region of dynamically “young” structures. Groups of galaxies are located in the region of low concentration of galaxies and large magnitude gaps $\Delta M_{1,4}$, i.e., in the region of dynamically “old” structures.

3.3. Dependences of the R_{sp}/R_{200} ratio on L_X , M_{200}

In Section 1 we quoted the results of More et al.(2015), which imply that the R_{sp} radius de-

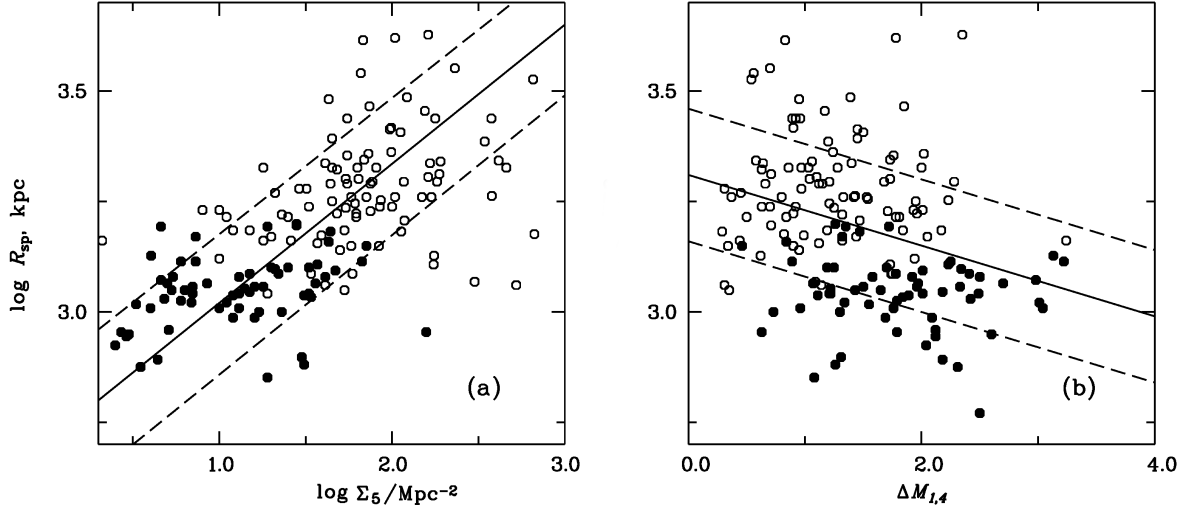


Figure 6. Dependence of radius R_{sp} (a) on galaxy concentration Σ_5 , (b) on magnitude gap $\Delta M_{1,4}$ between the first and fourth brightest galaxies within $0.5 R_{200}$. The filled circles show groups of galaxies with $\sigma \leq 400 \text{ km s}^{-1}$. The solid lines show the regression relations $R_{\text{sp}} \propto \Sigma_5^{0.31}$ and $R_{\text{sp}} \propto 10^{-0.08 \Delta M_{1,4}}$. The dashed lines show the 1σ deviations from these relations.

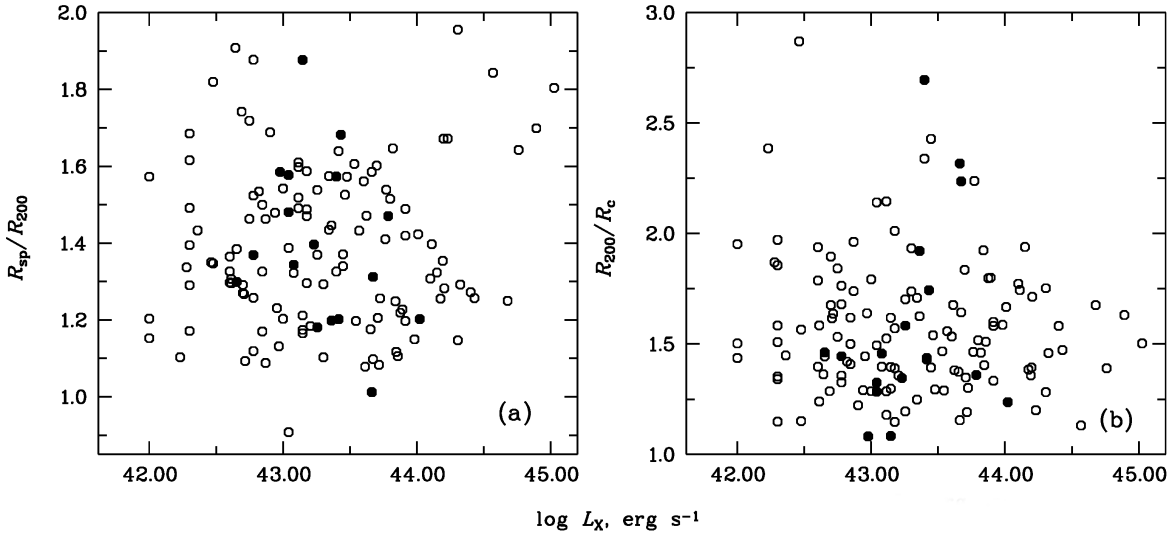


Figure 7. Dependence of the R_{sp}/R_{200} (a) and R_{200}/R_c (b) ratios on the 0.1–2.4 keV X-ray luminosity. The filled circles show groups and clusters of galaxies with bimodal distribution of line-of-sight velocities.

depends on the dark-matter accretion rate onto the cluster: in the case of high accretion rate this radius is close to the virial radius, i.e., in our case, it is close to R_{200} . Fig. 7 shows the dependences of the R_{sp}/R_{200} and R_{200}/R_c radius ratios on the X-ray luminosity of groups/clusters of galaxies.

Fig. 7 shows that our sample of systems of

galaxies appears rather compact on the diagram and that the R_{sp}/R_{200} ratio varies approximately from 1 to 2. We found that this ratio ranges from 1.15 to 1.6 for the bulk of clusters with $\log L_X \in [42.5; 44.5]$. Groups and clusters of galaxies with the radius ratios less than 1.15 (or $R_{\text{sp}}/R_{200\text{m}} < 0.72$) (see Fig. 7) can be classi-

fied as structures with high mass accretion rates (FA), and those with the radius ratios greater than 1.6 (or $R_{\text{sp}}/R_{200\text{m}} > 1.00$), as structures with slow accretion rates (SA). As is evident from Fig. 7, only two groups are located below $R_{\text{sp}}/R_{200} \sim 1.08$, i.e., the actual boundary is at about 1.08. Our approximate boundaries are somewhat smaller compared to the the results of simulations performed by More et al. (2015). Our sample of 157 objects contains 19 FA and 22 SA groups and clusters of galaxies. FA structures are mostly clusters of galaxies with non-Gaussian distribution of line-of-sight velocities, signs of mergers with other groups and galaxies near the virial radius, e.g., A 1270, A 1904, A 1991, and NGC 2563. Among SA clusters of galaxies there are rich clusters, such as A 1656, A 1795, A 2142, and A 2029, and poor groups, such as NGC 7237, IC 2476, MCG-01-29, which accrete matter (groups, galaxies, and gas) from large clustercentric distances.

4. CONCLUSIONS

Groups and clusters of galaxies have no clear boundaries because of the permanent infall of neighboring groups of galaxies, galaxies, gas, and dark-matter particles. Therefore determination of their boundaries always remains an issue of great importance despite the use of known methods that involve a comparison of the distribution of galaxies with results of simulations or application of the virial theorem to the cluster. In this paper we report the new observed boundaries of the groups and clusters of galaxies inferred from the galaxies, which we identify with the splashback radius R_{sp} equal to the radius of the apocenters of most of the accreted galaxies. We use our sample of 157 galaxies (based on SDSS data) from the local Universe with redshifts $0.01 < z < 0.10$ and masses $2 \times 10^{13} M_{\odot} < M_{200} < 2.5 \times 10^{15} M_{\odot}$. We analyzed the observed profiles of these groups and clusters of galaxies and determined the radii R_{sp} and R_c (the radius of the central region) and studied dependences of these radii on other properties of groups and clusters. We reconstructed the observed (projected) profile of each group of

cluster of galaxies—the integrated distribution of the number of all galaxies and early-type galaxies as a function of the squared distance from the center. This profile shows a steep increase of the number of galaxies, which then becomes linear. We used the transition point to find $R_{\text{sp}} > R_{200}$. We used the steepest part of this profile to estimate the radius R_c of the central region of each structure. We studied how R_{sp} and R_c depend on such properties of groups and clusters of galaxies as their X-ray luminosity, dynamical mass M_{200} inferred from σ , K -band luminosity ($M_K < -21^{\text{m}}$), concentration of galaxies Σ_5 , and the degree to which the brightest galaxy is distinguished, $\Delta M_{1,4}$.

We obtained the following results:

1. The boundary of the dark halo of groups and clusters of galaxies (the R_{sp} radius) determined from galaxies is proportional to the radius R_{200} of the virialized part estimated from the dispersion of line-of-sight velocities and to the radius R_c of the central virialized part. We found that $R_{\text{sp}} \propto R_{200}$ and $R_{\text{sp}} \propto R_c^{0.95 \pm 0.05}$.
2. All our measured radii correlate with X-ray luminosity and the dependences have similar slopes. We found the smallest scatter for the dependence of the splashback radius on X-ray luminosity: $R_{\text{sp}} \propto L_X^{0.24 \pm 0.03}$ (rms = 0.092). We also found that $R_c \propto L_X^{0.26 \pm 0.04}$ (rms = 0.110) and $R_{200} \propto L_X^{0.25 \pm 0.03}$ (rms = 0.097). The dependences of the splashback radius on mass M_{200} and $L_{K,200}$ have even smaller scatter.
3. Note that the R_{sp}/R_{200} ratio (Fig. 7) for most of the groups and clusters of galaxies varies within a narrow interval from 1 to 2. However, according to simulations More et al. 2015), types of objects with high and low rates of accretion from the surrounding space can be identified. We classified 19 groups and clusters as FA structures ($R_{\text{sp}}/R_{200} \leq 1.15$), and measured $\langle R_{\text{sp}} \rangle = 1.42 \pm 0.10$. We also classified 22 groups and clusters of galaxies as SA structures ($R_{\text{sp}}/R_{200} \geq 1.60$) with $\langle R_{\text{sp}} \rangle = 2.22 \pm 0.23$.
4. We found a weak dependence of the radius R_{sp} of groups and clusters of galaxies on the magnitude gap between the first and fourth brightest galaxies, $\Delta M_{1,4}$, inside the $0.5 R_{200}$ radius.

ACKNOWLEDGMENTS

This research has made use of the NASA/IPAC Extragalactic Database (NED, <http://nedwww.ipac.caltech.edu>), which is operated by the Jet Propulsion Laboratory, California Institute of Technology, under contract with the National Aeronautics and Space Administration, Sloan Digital Sky Survey (SDSS, <http://www.sdss.org>), which is supported by Alfred P. Sloan Foundation, the partic-

ipant institutes of the SDSS collaboration, National Science Foundation, and the United States Department of Energy and Two Micron All Sky Survey (2MASS, <http://www.ipac.caltech.edu/2mass/releases/allsky/>).

CONFLICT OF INTEREST

The authors declare that there is no conflict of interest.

-
1. S. Adhikari, N. Dalal, and R. T. Chamberlain, *J. Cosmology and Astroparticle Physics* **11**, 19 (2014).
 2. S. Adhikari, N. Dalal, and J. Clampitt, *J. Cosmology and Astroparticle Physics* **07**, 22 (2016).
 3. M. L. Balogh, J. F. Navarro, and S. L. Morris, *Astrophys. J.* **540**, 113 (2000).
 4. E. Baxter, C. Chang, B. Jain, et al., *Astrophys. J.* **841**, 18 (2017).
 5. H. Böhringer, W. Voges, J. P. Huchra et al., *Astrophys. J. Suppl.* **129**, 435 (2000).
 6. H. Böhringer, P. Schuecker, L. Guzzo et al., *Astronom. and Astrophys.* **425**, 367 (2004).
 7. P. Busch and S. D. M. White, *Monthly Notices Roy. Astronom. Soc.* **470**, 4767 (2017).
 8. R. G. Carlberg, H. K. C. Yee, E. Ellingson, et al., *Astrophys. J.* **485**, L13 (1997).
 9. C. Chang, E. Baxter, B. Jain, et al., *Astrophys. J.* **864**, 83 (2018).
 10. O. Contigiani, H. Hoekstra, and Y. M. Bahé, *Monthly Notices Roy. Astronom. Soc.* **485**, 408 (2019).
 11. B. Diemer and A. V. Kravtsov, *Astrophys. J.* **789**, 1 (2014).
 12. H. Ebeling, A. C. Edge, H. Böhringer et al., *Monthly Notices Roy. Astronom. Soc.* **301**, 881 (1998).
 13. H. Ebeling, C. R. Mullis, R. B. Tully, *Astrophys. J.* **580**, 774 (2002).
 14. M. Fong and J. Han, *Monthly Notices Roy. Astronom. Soc.* **503**, 4250 (2021).
 15. S. P. D. Gill, A. Knebe, and B. K. Gibson, *Monthly Notices Roy. Astronom. Soc.* **356**, 1327 (2005).
 16. J. E. Gunn and R. J. III Gott *Astrophys. J.* **176**, 1 (1972).
 17. R. J. III Gott, *Astrophys. J.* **186**, 481 (1973).
 18. C. P. Haines, M. J. Pereira, G. P. Smith, et al., *Astrophys. J.* **806**, 101 (2015).
 19. A. I. Kopylov and F. G. Kopylova, *Astrophysical Bulletin* **62**, 311 (2007).
 20. F. G. Kopylova and A. I. Kopylov, *Astrophysical Bulletin* **74**, 1 (2009).
 21. A. I. Kopylov and F. G. Kopylova, *Astrophysical Bulletin* **65**, 205 (2010).
 22. F. G. Kopylova and A. I. Kopylov, *Astron. Lett.* **37**, 257 (2011).
 23. A. I. Kopylov and F. G. Kopylova, *Astrophysical Bulletin* **67**, 17 (2012).
 24. F. G. Kopylova and A. I. Kopylov, *Astron. Lett.* **39**, 1 (2013).
 25. A. I. Kopylov and F. G. Kopylova, *Astrophysical Bulletin* **70**, 243 (2015).
 26. F. G. Kopylova and A. I. Kopylov, *Astrophysical Bulletin* **71**, 257 (2016).
 27. F. G. Kopylova and A. I. Kopylov, *Astrophysical Bulletin* **72**, 100 (2017).
 28. F. G. Kopylova and A. I. Kopylov, *Astrophysical Bulletin* **73**, 267 (2018).
 29. F. G. Kopylova and A. I. Kopylov, *Astrophysical Bulletin* **74**, 365 (2019).
 30. M. J. Ledlow, W. Voges, F. N. Owen, and J. O. Burns, *Astronom. J.* **126**, 2740 (2003).
 31. A. Mahdavi, H. Böhringer, M. J. Geller, and M. Ramella, *Astrophys. J.* **534**, 114 (2000).
 32. G. A. Mamon, T. Sanchis, E. Salvador-Sole, and J. M. Solanes, *Astronom. and Astrophys.* **414**, 445 (2004).
 33. S. More, B. Diemer, and A. V. Kravtsov, *Astrophys. J.* **810**, 36 (2015).
 34. S. More, H. Miyatake, M. Takada, et al., *Astrophys. J.* **825**, 39 (2016).
 35. J. S. Mulchaey, D. S. Davis, R. F. Mushotsky, and D. Burstein, *Astrophys. J. Suppl.* **145**, 39 (2003).
 36. K. A. Pimbblet, *Monthly Notices Roy. As-*

- tronom. Soc.**411**, 2637 (2010).
37. T. Shin, S. Adhikari, E. J. Baxter, et al., Monthly Notices Roy. Astronom. Soc.**487**, 2900 (2019).
38. K. Umetsu and B. Diemer, Astrophys. J. **836**, 231 (2017).
39. D. Zürcher and S. More, Astrophys. J. **874**, 184 (2019).

Translated by A. Dambis